Basal forebrain mediates prosocial behavior via disinhibition of midbrain dopamine neurons

Jun Wang[a,b,c,1], Jie Li[a,b,c,1], Qian Yang[a,b,c,1], Ya-Kai Xie[a,b,c], Ya-Lan Wen[a,b,c], Zhen-Zhong Xu[a,b,c], Yulong Li[d], Tianle Xu[e], Zhi-Ying Wu[a,b,c], Shumin Duan[a,b,c], and Han Xu[a,b,c,2]

[a]Department of Neurology of the Second Affiliated Hospital, Zhejiang University School of Medicine, Hangzhou 310058, China; [b]Department of Neurobiology, Zhejiang University School of Medicine, Hangzhou 310058, China; [c]NHC and CAMS Key Laboratory of Medical Neurobiology, MOE Frontier Science Center for Brain Research and Brain-Machine Integration, School of Brain Science and Brain Medicine, Zhejiang University, Hangzhou 310058, China; [d]State Key Laboratory of Membrane Biology, Peking University School of Life Sciences, PKU-IDG/McGovern Institute for Brain Research, Peking-Tsinghua Center for Life Sciences, Beijing 100871, China; and [e]Center for Brain Science and Department of Anatomy and Physiology, Shanghai Jiao Tong University School of Medicine, Shanghai 200025, China

Sociability is fundamental for our daily life and is compromised in major neuropsychiatric disorders. However, the neuronal circuit mechanisms underlying prosocial behavior are still elusive. Here we identify a causal role of the basal forebrain (BF) in the control of prosocial behavior via inhibitory projections that disinhibit the midbrain ventral tegmental area (VTA) dopamine (DA) neurons. Specifically, BF somatostatin-positive (SST) inhibitory neurons were robustly activated during social interaction. Optogenetic inhibition of these neurons in BF or their axon terminals in the VTA largely abolished social preference. Electrophysiological examinations further revealed that SST neurons predominantly targeted VTA GABA neurons rather than DA neurons. Consistently, optical inhibition of SST neuron axon terminals in the VTA decreased DA release in the nucleus accumbens during social interaction, confirming a disinhibitory action. These data reveal a previously unappreciated function of the BF in prosocial behavior through a disinhibitory circuitry connected to the brain's reward system.

basal forebrain | disinhibition | social interaction | ventral tegmental area

Prosocial behavior is of great importance to our daily life and represents the cornerstone of human society (1, 2). Conversely, impairments in social cognition and social interaction are commonly observed in a number of neuropsychiatric disorders, notably autism spectrum disorders (ASDs) (3, 4). However, in striking contrast to a rapid increase in the number of individuals afflicted, the effective treatment options for social deficits remain inadequate. Essentially, a deeper mechanistic understanding of social behavior and social impairment is currently needed.

Since the concept of "the social brain" was coined in the late 20th century (5, 6), the study of social neuroscience has thrived. A growing body of studies from both human beings and animals of different species have been conducted to unravel the mystery behind social behavior at multiple levels varying from molecules to circuits (7–12). Not surprisingly, mirroring the complex nature of social behavior, a number of brain regions have been discovered to be involved in the process of social perception, social cognition, and social interaction over the past decades (13–22). Among many mechanistic understandings of social behavior, one outstanding advance in recent years is the recognition that the brain's reward system plays a critical role in prosocial interaction behavior (14, 16, 17, 19). Particularly, the projection from the midbrain ventral tegmental area (VTA) dopamine (DA) neurons to the nucleus accumbens (NAc) is found to produce a rewarding effect and to mediate prosocial behavior in mice (14). However, the neural mechanism by which social information is relayed to the VTA, which leads to control of social behavioral manifestation, is still elusive.

The basal forebrain (BF) is a collection of brain structures located in the rostroventral forebrain and was traditionally defined by the presence of cholinergic projection neurons (23). Accordingly, previous studies have been mostly focused on cholinergic neurons and have revealed essential roles of this neuronal population in the

regulation of arousal, attention, learning, and memory (24–26). In addition to cholinergic neurons, the BF also comprises other major neuronal types including glutamatergic neurons and GABAergic neurons expressing either somatostatin (SST) or parvalbumin (PV) (27, 28). Recently, a diversity of brain functions has started to be unraveled for the noncholinergic neuronal types in the BF as well. For example, BF SST inhibitory neurons promote high-calorie food intake (29), yet glutamatergic neurons drive food avoidance through projections to the lateral hypothalamus (30). Also, cortically projecting BF PV inhibitory neurons regulate cortical gamma band rhythms (31). However, the functional role of the BF in social behavior and its neuronal substrate has not been investigated.

Neuronal structure abnormalities in the BF have been identified in patients with ASDs, which are characterized by severe impairments in social cognition and interaction (32–34). Consistently, brain-imaging studies have also highlighted functional reduction of the BF in low-functioning autistic children (35). Does the BF play a causal role in social behavior? Also, what is the neuronal circuitry behind this mechanism? These are significant questions to be explored. Recent neural tracing studies with advanced viral genetic tools reveal dense anatomical connections between the BF and the VTA (36–38). Thus, we hypothesized that the BF projections to the VTA may carry information important for prosocial behavior.

Significance

The basal forebrain (BF) is traditionally recognized as a brain structure crucial for arousal, attention, learning, and memory. Here, we discovered a causal role of the BF in the control of prosocial behavior, which is fundamental for our daily life. We showed in mice that the BF somatostatin-expressing inhibitory neurons predominantly target GABA neurons and disinhibit dopamine neurons in the ventral tegmental area and thereby increase dopamine release in the nucleus accumbens. This disinhibitory circuitry played an essential role in promoting social interaction behavior. Our findings identify a previously unknown function of the BF in social behavior regulation and suggest a potential therapeutic target for social deficits commonly observed in major neuropsychiatric disorders.

NEUROSCIENCE

www.manaraa.com

Results

BF SST Neurons Are Activated during Social Interaction. The BF comprises four major neuronal subpopulations, of which both the vesicular glutamate transporter 2 (vGluT2)-expressing glutamatergic neurons and the SST-expressing GABAergic neurons densely project to the VTA (36), one key brain region that is critical for reward processing and social behavior (14). To confirm this anatomic organization, we injected vGluT2-Cre mice (39) and SST-Cre
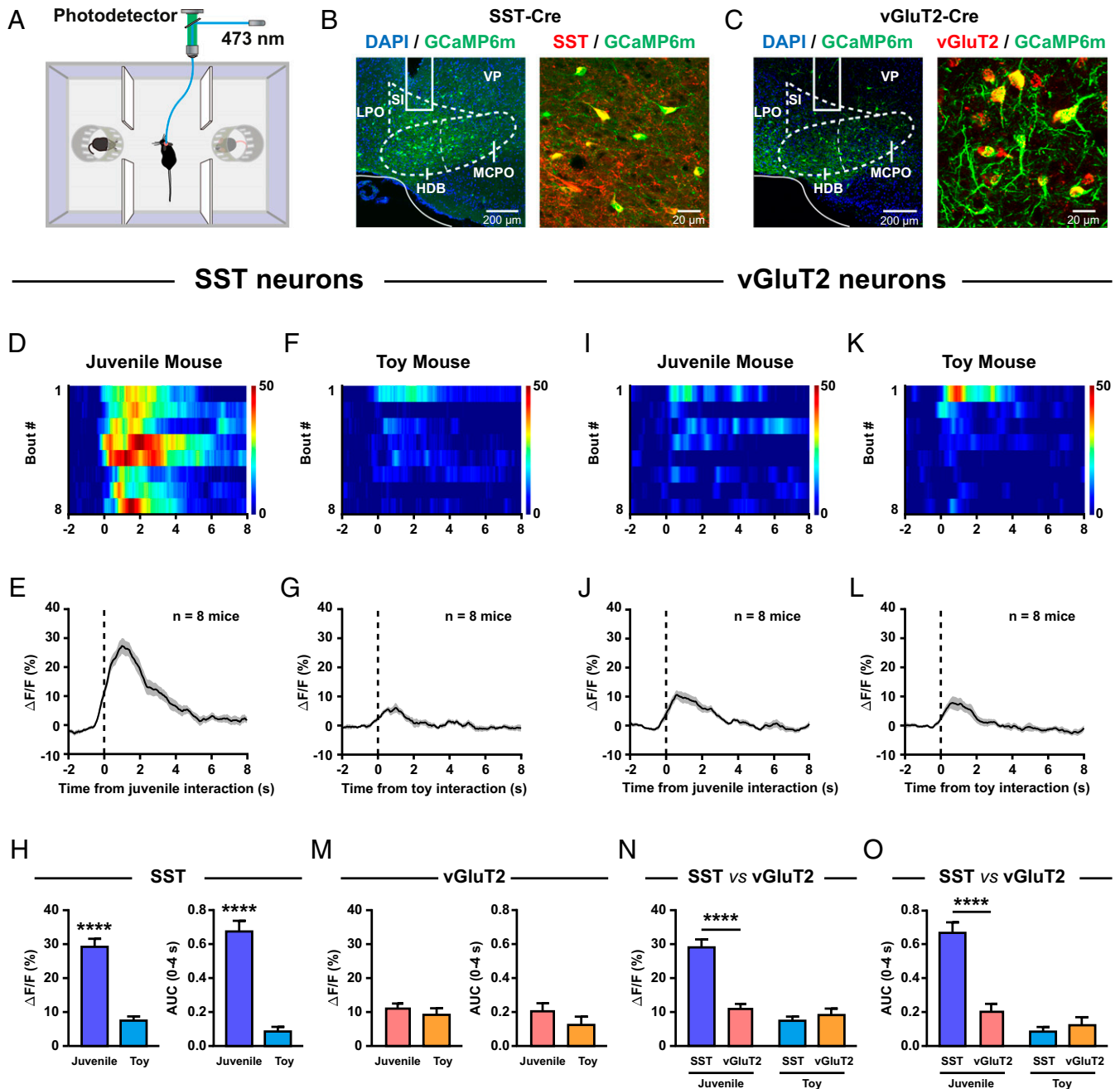

Fig. 1. BF SST neurons are robustly activated during social interaction. (*A*) Schematic diagram of the fiber photometry setup. Ca²⁺ transients were recorded from GCaMP6m-expressing SST neurons or vGluT2 neurons of mice subjected to the three-chamber social interaction task. (*B*, *Left*): placement of an optic fiber for fiber photometry in the BF of a SST-Cre mouse injected with GCaMP6m. (*Right*) GCaMP6m expression in BF SST neurons. DAPI, 4′,6-diamidino-2-phenylindole; HDB, the horizontal limb of the diagonal band; LPO, lateral preoptic area; MCPO, magnocellular preoptic nucleus; SI, substantia innominata; VP, ventral pallidum. (*C*) The same as *B* but for the vGluT2-Cre mouse. (*D*) Ca²⁺ signals of a SST-Cre mouse were activated during juvenile mouse interaction. The heatmap illustration of Ca²⁺ signals was aligned to the onset of individual interactions. Note that time 0 was defined as the time point when the experimental mouse was closest to the stimulus mouse. Each row represents one bout, and a total of eight bouts are illustrated. The color scale at the right indicates ΔF/F. (*E*) The peri-event plot of the mean Ca²⁺ transient during juvenile mouse interaction for the entire test group (*n* = 8 mice). The thick line indicates the mean, and the shaded area indicates SEM. (*F* and *G*) The same as *D* and *E* but for toy mouse interaction. (*H*) Statistical comparison of fluorescence signals (*Left*: peak amplitude; *Right*: AUC) of BF SST neurons between juvenile mouse interaction and toy mouse interaction. ****$P < 0.0001$, paired *t* test. Error bars indicate mean ± SEM. (*I–M*) The same as *D–H* but for vGluT2 neurons. (*N*) Statistical comparison of the peak amplitude of fluorescence signals between BF SST neurons and BF vGluT2 neurons. (*Left*) Juvenile mouse interaction. (*Right*) Toy mouse interaction. ****$P < 0.0001$, two-way ANOVA followed by Bonferroni post hoc analysis. Error bars indicate mean ± SEM. (*O*) The same as *N* but for the AUC of fluorescence signals.

www.manaraa.com

mice (40) with anterograde synaptic tracer AAV2/9-hSyn-FLEX-membrane green fluorescent protein (mGFP)-Synaptophysin-mRuby (SYP:mRuby) in the BF (*SI Appendix*, Fig. S1). Consistent with previous findings, we observed dense SYP:mRuby puncta in the VTA from both GABAergic and glutamatergic inputs. Furthermore, we found that GABAergic fibers showed significantly differential innervation along the rostral-caudal axis of the VTA, with the greatest density of SYP:mRuby puncta detected in the rostral VTA (VTAR) (*SI Appendix*, Fig. S1).

To probe whether and how BF vGluT2 neurons and SST neurons respond to social stimuli, we sought to directly measure their activities during real-time social interaction with fiber photometry. We used a three-chamber social interaction test, a well-established experimental paradigm to analyze social behavior in rodents (Fig. 1*A*) (41, 42). Following stereotaxic infusion of the Cre-inducible AAV-DIO-GCaMP6m into the BF of SST-Cre or vGluT2-Cre knock-in mice, a small optical fiber was implanted for chronic recording of GCaMP6m fluorescence signals. The efficiency and specificity of GCaMP6m expression in SST neurons (Fig. 1*B*) and vGluT2 neurons (Fig. 1*C*) were verified with immunohistochemistry and RNAscope in situ hybridization, respectively.

We first examined the neuronal activities of BF SST neurons. There was a robust increase in fluorescence signals each time the experimental mice interacted with a juvenile stimulus mouse (Fig. 1 *D* and *E*). It is likely that the experimental mice were able to detect sensory cues of the stimulus mouse when they were approaching the stimulus mouse since the photometric signals preceded the interaction onset, that is, when the experimental mice were closest to the stimulus mouse. As a comparison, a minimal increase in fluorescence signals was observed when these mice interacted with a toy mouse (Fig. 1 *F* and *G*). Indeed, both the peak amplitude and the area under curve (AUC) of fluorescence signals of SST neurons during social interaction with a juvenile mouse were significantly larger than those during a toy mouse investigation (Fig. 1*H*). In striking contrast, as for BF vGluT2 neurons, only a slight change in fluorescence signals was observed when the experimental mice interacted with either a juvenile mouse (Fig. 1 *I* and *J*) or a toy mouse (Fig. 1 *K* and *L*). Unlike the highly differential responses seen in SST neurons (Fig. 1*H*), the fluorescence signals of vGluT2 neurons were comparable between juvenile mouse investigation and toy mouse investigation (Fig. 1*M*). When the fluorescence signals were compared between SST neurons and vGluT2 neurons, we found that SST neurons were significantly more responsive to juvenile mouse stimuli than vGluT2 neurons were, although both SST neurons and vGluT2 neurons were similarly irresponsive to toy mouse stimuli (Fig. 1 *N* and *O*). In addition, significantly increased Ca^{2+} transients were also detected in SST neurons when the experimental mouse was interacting with an adult male or an adult female stimulus mouse (*SI Appendix*, Fig. S2). These observations indicate that the responses of BF SST neurons were not dependent on the age or sex of the stimulus animals. Together, these results demonstrate that BF SST neurons, but not vGluT2 neurons, were robustly activated during social interaction.

Inhibition of BF SST Neurons Impairs Prosocial Behavior. To determine whether the activities of BF SST neurons contribute to the expression of prosocial behavior, we optogenetically inhibited these neurons and examined the consequence of the inhibition on sociability. For this purpose, SST-Cre mice were injected with a Cre-dependent AAV expressing enhanced yellow fluorescent protein (EYFP)-tagged eNpHR3.0 and implanted with optical fibers bilaterally in the BF (Fig. 2*A*). Immunohistochemical analysis verified the efficiency and selectivity of halorhodopsin (NpHR)-EYFP expression in SST neurons (Fig. 2*B*). Photostimulation

(589 nm, 250 ms, 5 to 10 mW) efficiently hyperpolarized infected SST neurons and completely suppressed their firing activities evoked by current injections (Fig. 2*C*).

Next, we optogenetically inhibited BF SST neurons each time the experimental mice entered the social chamber as the mice performed the three-chamber social interaction task (Fig. 2*D*). Mice are social animals, and they typically spend a majority of their time exploring the social chamber and social zone (Fig. 2*E*) (41, 42). However, as compared to the control SST-Cre mice expressing EYFP, those expressing NpHR spent significantly less time in the social chamber (Fig. 2*F*) and social zone (Fig. 2*J*). Strikingly, when BF SST neurons were optically inhibited, the mice did not show a preference for social chamber any more (Fig. 2*F*). Accordingly, the social index was significantly reduced in NpHR mice as well (Fig. 2 *G* and *K*). A closer inspection further revealed that inhibition of SST neurons did not affect entry times of either social chamber (Fig. 2*H*) or social zone (Fig. 2*L*), but significantly reduced the mean duration of individual visits of the social chamber (Fig. 2*I*) and social zone (Fig. 2*M*). These results demonstrate that inhibition of BF SST neurons impairs normal sociability.

Mice would also spend less time in the social chamber if inhibition of BF SST neurons produced an aversive effect. To clarify this possibility, we examined the consequence of inhibiting BF SST neurons with the real-time place avoidance paradigm. Mice were allowed to freely explore a two-chamber apparatus, and yellow light was delivered each time the experimental mice entered a randomly assigned chamber (*SI Appendix*, Fig. S3 *A* and *B*). Both EYFP mice and NpHR mice spent an equal amount of time in the light-on and light-off chambers, suggesting that inhibition of BF SST neurons was not aversive (*SI Appendix*, Fig. S3 *C* and *D*). In addition, optogenetic inhibition of BF SST neurons did not affect either locomotion or general anxiety of the mice assessed with an open field test (*SI Appendix*, Fig. S3 *E–I*). Therefore, these results indicate that BF SST neurons are indeed required for the mice to show normal prosocial behavior.

Inhibition of the BF SST→VTA Pathway Impairs Social Interaction. Among multiple downstream targets of BF SST neurons, the VTA represents a key hub for motivation and social behavior (14). To know whether the BF SST neurons that project to VTA have a causal role in prosocial interaction behavior, we selectively inhibited the pathway with optogenetics. Specifically, we virally expressed EYFP-tagged eNpHR3.0 in BF SST neurons and implanted optical fibers bilaterally in the VTA (Fig. 3 *A* and *B*). Six weeks later, dense EYFP-labeled fibers were readily visible in the VTA (Fig. 3*C*). The functional effectiveness of terminal suppression by optogenetic manipulation was verified with in vitro patch clamp recordings in VTA neurons. The frequency of spontaneous inhibitory postsynaptic currents (sIPSCs) in GABAergic neurons was significantly reduced during yellow light stimulation (*SI Appendix*, Fig. S4 *A–C*). These results demonstrate that GABA release was indeed suppressed by optogenetic inhibition of the BF SST→VTA projections. Next we optogenetically inhibited the axon terminals of BF SST neurons in the VTA each time the experimental mice entered the social chamber in a three-chamber social interaction test (Fig. 3*D*). Similar to the effect of direct inhibition of BF SST cell bodies, BF SST-VTA:NpHR mice spent significantly less time in the social chamber and social zone compared with EYFP control mice (Fig. 3 *E*, *F*, and *J*). The social index of BF SST-VTA:NpHR mice was significantly smaller than that of EYFP control mice (Fig. 3 *G* and *K*). Again, inhibition of the BF SST→VTA pathway did not alter entry times (Fig. 3 *H* and *L*) but significantly decreased the mean duration of individual explorations of the social chamber (Fig. 3*I*) and social zone (Fig. 3*M*). Moreover, the same

Wang et al.
Basal forebrain mediates prosocial behavior via disinhibition of midbrain dopamine neurons
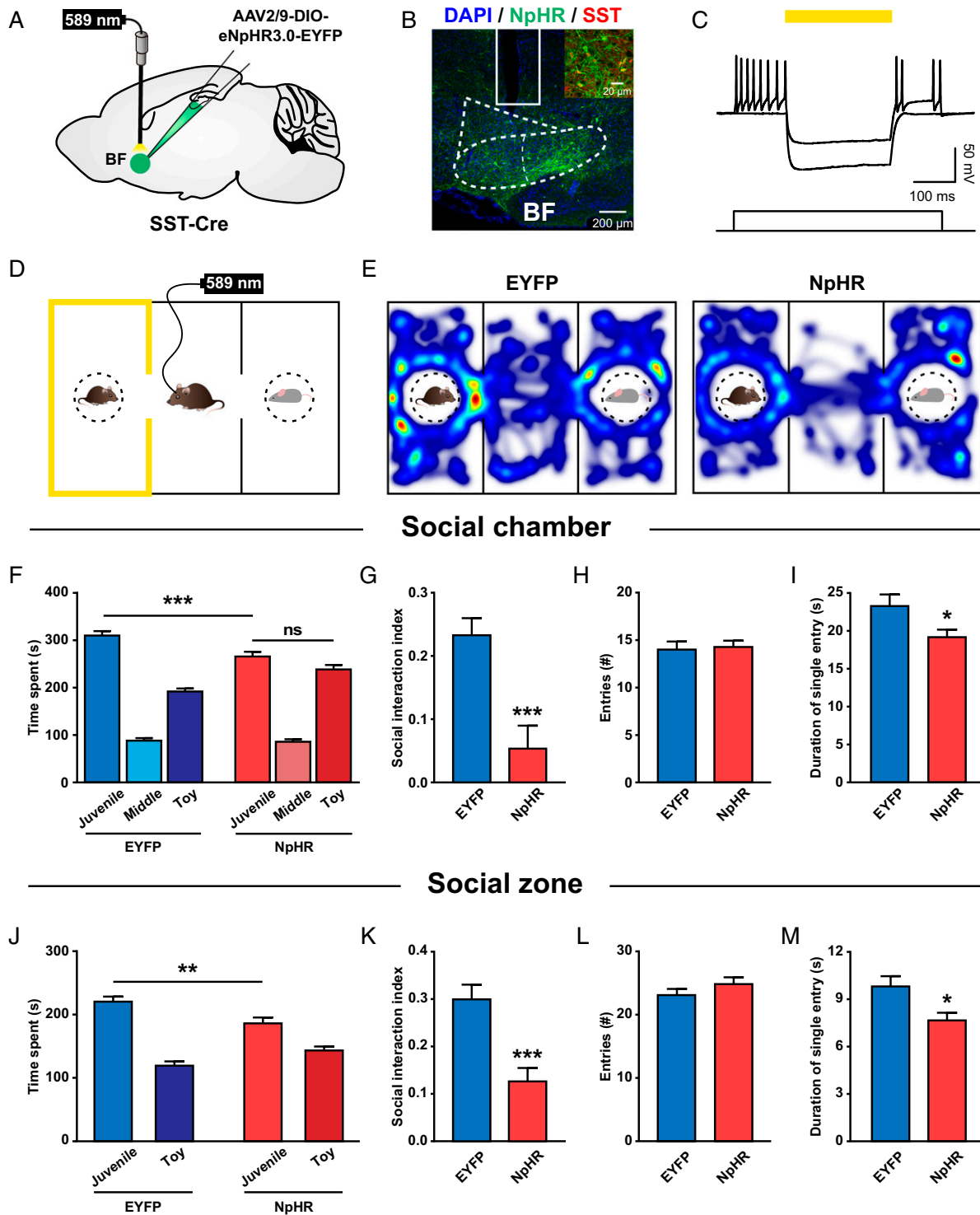
www.manaraa.com

Fig. 2. Optogenetic inhibition of BF SST neurons impairs prosocial behavior. (*A*) Schematic illustration of eNpHR3.0-EYFP virus injection and optical fiber implantation in the BF. (*B*) Representative image showing virus expression and optical fiber placement in the BF. (*Inset*) Colocalization of NpHR expression (green) and SST staining (red). (*C*) Yellow light induced a large amplitude hyperpolarization in an NpHR-expressing SST neuron and suppressed its spiking activities evoked by current injection. (*D*) Schematic illustration of an experimental mouse subjected to a three-chamber social interaction test, where social chamber was paired with constant yellow light stimulation (589 nm, 5 to 8 mW). (*E*) Representative heatmaps showing the locations of an EYFP-expressing control mouse (*Left*) and an NpHR-expressing experimental mouse (*Right*) in a three-chamber social interaction test. (*F*) Quantification of the time spent by EYFP and NpHR mice in each chamber. Note that NpHR mice spent significantly less time in the social chamber compared to EYFP mice. ***$P < 0.001$; ns, $P > 0.05$; two-way ANOVA followed by Bonferroni post hoc analysis. (*G*) The social interaction index (the difference in the time spent in the social and neutral chambers divided by the total time spent in both chambers) was significantly smaller in NpHR mice. ***$P < 0.001$; unpaired t test. (*H*) There was no difference in the number of entries into the social chamber between EYFP and NpHR mice. (*I*) The mean duration of individual social chamber investigations was significantly shorter in NpHR mice. *$P < 0.05$; unpaired t test. (*J–M*) The same as *F–I* but for the time spent in each zone (5-cm vicinity of the social or neutral cage). *$P < 0.05$; **$P < 0.01$; ***$P < 0.001$. Error bars indicate mean $\pm$ SEM (EYFP, $n = 15$; NpHR, $n = 15$).
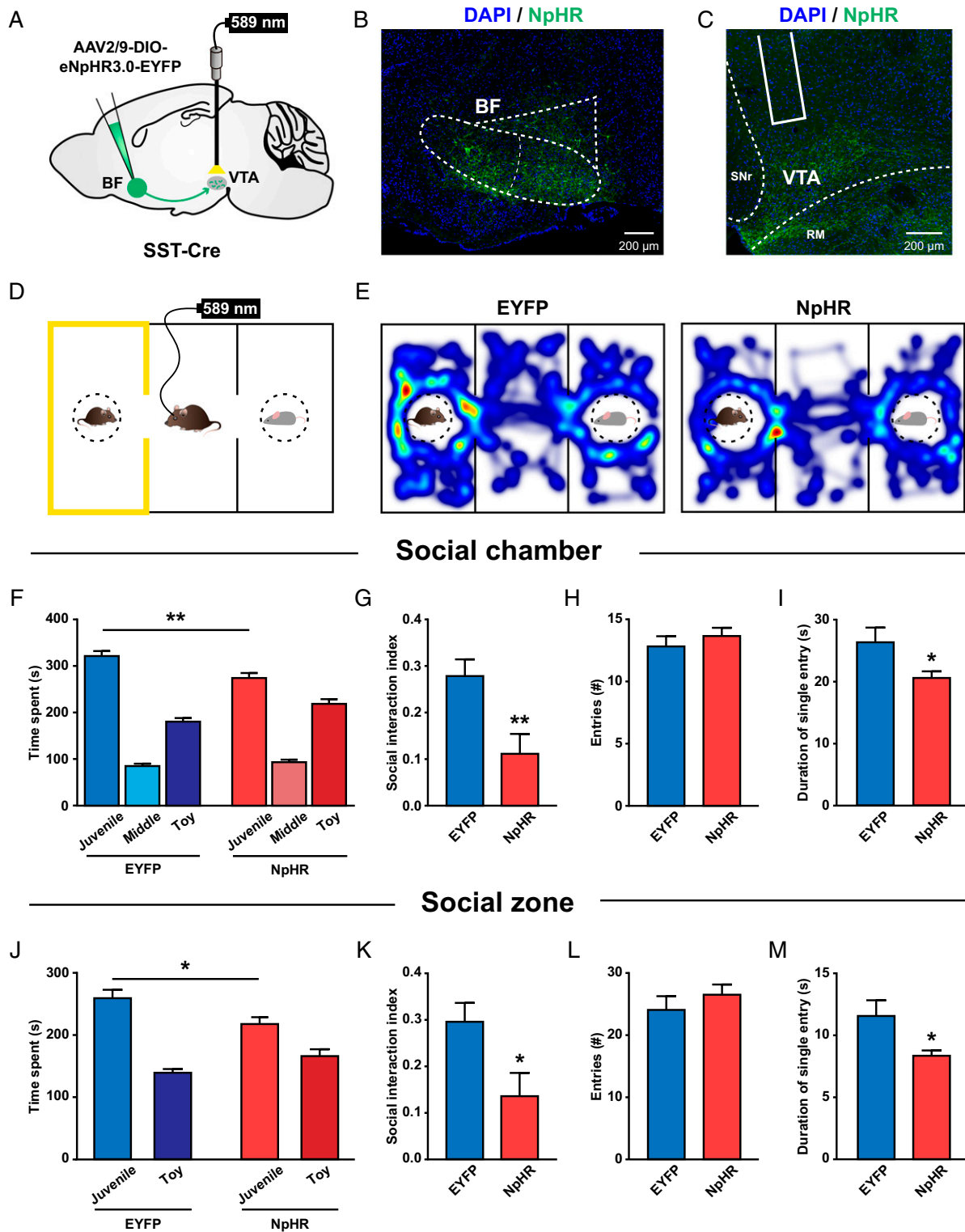
Social chamber

Social zone

Fig. 3. Optogenetic inhibition of BF SST→VTA pathway impairs social interaction. (*A*) Schematic illustration of eNpHR3.0-EYFP virus injection in the BF and optical fiber implantation in the VTA. (*B* and *C*) Representative images showing NpHR expression in the BF (*B*) and NpHR-expressing axon terminals in the VTA (*C*). SNr, substantia nigra, reticular part; RM, retromammillary nucleus. (*D*) Schematic illustration of an experimental mouse subjected to a three-chamber social-interaction test, where the social chamber was paired with constant yellow light stimulation (589 nm, 5 to 8 mW). (*E*) Representative heatmaps showing the locations of an EYFP-expressing control mouse (*Left*) and an NpHR-expressing experimental mouse (*Right*) in a three-chamber social-interaction test. (*F*) Quantification of the time spent by EYFP and NpHR mice in each chamber. Note that NpHR mice spent significantly less time in the social chamber compared to EYFP mice. **$P < 0.01$; two-way ANOVA followed by Bonferroni post hoc analysis. (*G*) The social interaction index was significantly smaller in NpHR mice. **$P < 0.01$; unpaired t test. (*H* and *I*) There was no difference in the number of entries into the social chamber between EYFP and NpHR mice (*H*); however, the mean duration of individual social chamber investigations was significantly shorter in NpHR mice (*I*). *$P < 0.05$; unpaired t test. (*J*–*M*) The same as *F*–*I* but for the time spent in each zone. *$P < 0.05$. Error bars indicate mean ± SEM (EYFP, $n = 10$; NpHR, $n = 11$).

Wang et al.
Basal forebrain mediates prosocial behavior via disinhibition of midbrain dopamine neurons

optical inhibition did not produce an aversive effect and did not alter locomotion or general anxiety in BF SST-VTA:NpHR mice (*SI Appendix,* Fig. S5). Together, these data demonstrate that projections from BF SST neurons to the VTA are necessary for the control of prosocial behavior.

It should be noted that, although our results support a pro-social function of the BF SST→VTA inhibitory pathway, our results do not limit the function of this pathway to other forms of reward processing. Indeed, in a three-chamber food preference test, we found that optogenetic inhibition of the BF SST→VTA projections slightly but significantly reduced the food preference in fasted mice (*SI Appendix,* Fig. S6). These data suggest that the BF SST→VTA GABAergic input might be generally important for motivation and reward including social interaction.

Except for the VTA, the lateral habenula (LHb) is another brain area that receives dense innervations from BF SST neurons (*SI Appendix,* Fig. S1) (36). Given the crucial importance of the LHb in emotional control, we wondered whether the BF SST→LHb pathway may also play a prosocial role. To this end, we virally expressed EYFP-tagged NpHR3.0 in BF SST neurons and implanted optical fibers bilaterally in the LHb (*SI Appendix,* Fig. S7 *A and B*). Six weeks later, dense EYFP-labeled fibers were readily visible in the LHb (*SI Appendix,* Fig. S7C). Then we optogenetically inhibited the axon terminals of BF SST neurons in the LHb each time the experimental mice entered the social chamber in a three-chamber social interaction test (*SI Appendix,* Fig. S7D). We found that inhibition of the BF SST→LHb pathway produced no effect on measurements of social interaction time, social interaction index, entry times, or mean duration of individual visits (*SI Appendix,* Fig. S7 *E–M*), although photostimulation of BF SST-LHb:NpHR terminals significantly reduced the frequency of sIPSCs recorded in LHb neurons (*SI Appendix,* Fig. S4 *D–F*). Thus, in contrast to the BF SST→VTA pathway, projections from BF SST neurons to the LHb did not seem to have an effect on prosocial behavior under our experimental conditions.

BF SST Neurons Predominantly Target VTA GABA Neurons. The activity of VTA DA neurons is positively correlated with social interaction, and inhibition of these neurons compromises social interaction behavior (14). Because BF SST neurons are GABAergic and thus produce an inhibitory effect on their postsynaptic neurons, they have a detrimental effect on social interaction if they directly inhibit VTA DA neurons. This appeared paradoxical to the prosocial role of the BF SST→VTA pathway observed in the above experiments (Fig. 3). However, in addition to DA neurons, around 35% of the total VTA neurons are local GABA neurons, which make functional synapses with VTA DA neurons and are able to inhibit DA neurons (43, 44). Therefore, we reasoned that BF SST neurons might preferentially inhibit the local VTA GABA neurons and hence disinhibit DA neurons.

To test the above hypothesis, we first examined the functional connectivity of BF SST neurons with VTA GABA neurons and DA neurons, respectively. Specifically, a Cre-dependent AAV carrying channelrhodopsin (AAV-DIO-ChR2-mCherry) was injected into the BF of SST-Cre mice (Fig. 4 *A* and *B*). Fresh brain slices containing the VTA were generated 6 wk after virus injection, and whole-cell patch clamp recordings were performed from neurons in the VTAR since BF SST neurons predominantly innervate the rostral part of the VTA (Fig. 4 *A* and *B*). Recorded neurons were classified into GABA neurons and DA neurons based on post hoc immunohistochemical staining with GABA and tyrosine hydroxylase (TH) antibodies, respectively (Fig. 4 *C* and *D*). Consistent with previous studies (45, 46), we observed that DA neurons typically exhibited a markedly larger hyperpolarization-activated current (I_h) compared to GABA neurons (Fig. 4 *E* and *F*). Quantitative analysis revealed that the

I_h current recorded in DA neurons was nearly 10 times as large as that in GABA neurons (GABA: 5.03 ± 1.08 pA, $n = 20$; DA: 49.04 ± 8.21 pA, $n = 16$; Mann–Whitney U test, $P < 0.0001$; Fig. 4G).

Photostimulation of ChR2-expressing fibers in the VTA reliably evoked postsynaptic currents (PSCs) in a portion of GABA or DA neurons (Fig. 4H). In addition, the $GABA_A$ receptor antagonist bicuculline (BIC, 10 μM) suppressed light-evoked PSCs by 96.8% (artificial cerebrospinal fluid [ACSF]: 245.38 ± 105.75 pA vs. BIC: 7.90 ± 5.17 pA, $n = 6$) in VTA GABA neurons and by 99.2% (ACSF: 50.03 ± 23.19 pA vs. BIC: 0.40 ± 0.40 pA, $n = 3$) in VTA DA neurons, respectively. These data demonstrate that the BF SST→VTA connection is primarily GABAergic. However, surprisingly, the amplitude of IPSCs recorded in GABA neurons was much larger than that recorded in DA neurons (GABA neuron: 278.20 ± 68.07 pA, $n = 14$; DA neuron: 26.25 ± 4.38 pA, $n = 4$; Mann–Whitney U test, $P = 0.025$; Fig. 4I). Furthermore, in addition to the large difference in synaptic strength, the percentage of responsive cells by photostimulation was almost three times higher in GABA neurons than in DA neurons (GABA neuron: 70%, 14 of 20 recordings; DA neuron: 25%, 4 of 16 recordings, Fisher's exact test, $P < 0.0001$; Fig. 4J). These functional analyses revealed that BF SST neurons predominantly target VTA GABA neurons rather than DA neurons in terms of both synaptic strength and connection probability (Fig. 4K).

Inhibition of BF SST→VTA Projections Reduces DA Release in the NAc during Social Interaction. The differential innervation pattern of BF SST neurons in VTA GABA neurons and DA neurons suggested that BF SST neurons could disinhibit VTA DA neurons. Therefore, we inferred that BF SST neuron activation by social stimuli contributes at least in part to the elevated activities of VTA DA neuron axon terminals observed in the NAc during social interaction (14). If this is the case, one would expect that inhibition of BF SST→VTA projections could disturb the disinhibitory circuitry and attenuate NAc DA efflux caused by social stimuli.

We directly tested this possibility in vivo when animals were performing a social interaction task. The BF SST→VTA projections were inhibited with optogenetics, and NAc DA release was monitored with fiber photometry by using an optimized genetically encoded DA sensor, $GRAB_{DA2m}$ (47, 48). To do so, a Cre-dependent AAV carrying mCherry-tagged NpHR was injected bilaterally in the BF of SST-Cre mice, and another non–Cre-dependent AAV carrying a conformationally sensitive circular-permutated EGFP (cpEGFP)-inserted $GRAB_{DA2m}$ was injected unilaterally in the NAc core (Fig. 5 *A* and *B*). Two optical fibers were implanted bilaterally in the VTA to deliver light and to inhibit BF SST neuron axon terminals, and another optical fiber was implanted in the NAc to measure DA release (Fig. 5 *A* and *B*). Six weeks after virus injection, mCherry-labeled SST cell bodies and fibers were readily visible in the BF and the VTA, respectively (Fig. 5 *C*, *Top* and *Middle*). Also, $GRAB_{DA2m}$-cpEGFP was efficiently expressed in NAc neurons (Fig. 5 *C*, *Bottom*). Virus injection sites and optical fiber placements of the entire experimental group were verified by post hoc examinations, and most recordings were made in the NAc core where dopamine release was measured (*SI Appendix,* Fig. S8).

Then we tested virus-infected animals in an open field arena, and light-on and light-off conditions were alternated among trials when experimental mice were interacting with a juvenile stimulus mouse (Fig. 5D). As expected, in light-off trials, we observed a prominent increase in $GRAB_{DA2m}$ fluorescence signals each time experimental mice interacted with a juvenile stimulus mouse (Fig. 5 *E–G*). In addition, the increase in fluorescence signals was reliably coupled to the onset of each interaction behavior and maintained throughout the entire period until retreat from the stimulus mouse (Fig. 5 *F* and *G*). In
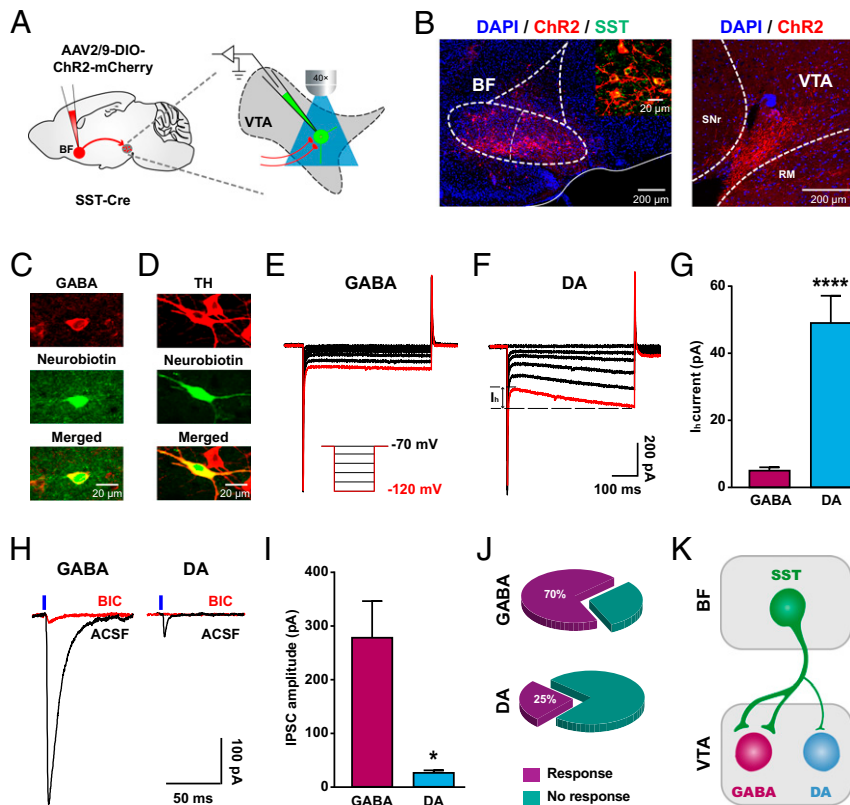
www.manaraa.com

Fig. 4. BF SST neurons preferentially inhibit VTA GABA neurons. (*A*) Schematic illustration of ChR2-mCherry virus injection in the BF and patch-clamp recording configuration in acute VTA slices. (*B*, *Left*) Representative image showing ChR2-mCherry expression in the BF. (*Inset*) Colocalization of ChR2 expression (red) and SST staining (green). (*Right*) Confocal image showing ChR2-expressing axon terminals in the VTA. (*C* and *D*) Neurons were filled with neurobiotin (green) during recording and subsequently identified as a GABA neuron or a DA neuron with immunostaining (red) for GABA (*C*) or TH (*D*), respectively. (*E* and *F*) Typical currents induced by hyperpolarizing voltage steps in a GABA neuron (*E*) and a DA neuron (*F*). Red traces represent currents induced by a hyperpolarizing voltage of −120 mV. (*Inset*) The experimental protocol of voltage-clamp recording (from −70 to −120 mV at -10-mV steps). (*G*) Quantification of hyperpolarization-activated currents (I_h) in response to a −120-mV voltage. Note that the I_h current of DA neurons is significantly larger than that of GABA neurons (GABA neuron, $n = 20$; DA neuron, $n = 16$). Error bars indicate mean ± SEM, ****$P < 0.0001$; Mann–Whitney U test. (*H*) Example IPSCs recorded in a GABA (*Left*) and a DA neuron (*Right*) by photostimulation of ChR2-expressing axon terminals in the VTA before (black) and after (red) bath application of 10 μM BIC. Blue vertical bars indicate the onset of light stimulation. (*I*) Quantification of the amplitude of light-evoked IPSCs. Note that IPSC amplitude was significantly greater in GABA neurons than in DA neurons (GABA neuron, $n = 14$; DA neuron, $n = 4$). Error bars indicate mean ± SEM, *$P < 0.05$; Mann–Whitney U test. (*J*) The percentage of recorded GABA neurons (*Top*) and DA neurons (*Bottom*) that were responsive to blue light stimulation. Note that the percentage of light-responsive GABA neurons was significantly greater than that of light-responsive DA neurons (GABA, 70% vs. DA, 25%; $P < 0.0001$; Fisher's exact test). (*K*) A schematic diagram illustrating preferential innervation of BF SST neurons in GABA neurons over DA neurons in the VTA.

comparison, fluorescence signals caused by social investigation were substantially reduced in light-on trials (Fig. 5 *H–J*). Statistical comparison revealed that both the peak amplitude and the AUC of GRAB$_{DA2m}$ fluorescence signals in response to social interaction were significantly smaller in light-on trials than in light-off trials (Fig. 5 *K* and *L*). It is noteworthy that the decrease in fluorescence signals was not an artifact caused by yellow light per se because no such reduction was noticed in mCherry-expressing control animals (*SI Appendix*, Fig. S9). Conversely, optogenetic activation of BF SST→VTA projections evoked a significant release of dopamine in the NAc (*SI Appendix*, Fig. S10). This observation further confirmed that BF SST→VTA projections are able to disinhibit VTA dopamine neurons and to increase dopamine release in the NAc. Together, these results were consistent with our hypothesis and indicate that BF SST neurons indeed disinhibited VTA DA neurons and promoted DA release in the NAc during real-time social interaction.

Discussion

In the present study, we report a previously unrecognized function of the BF in the control of social interaction behavior in mice. Furthermore, we demonstrate that the prosocial behavioral function was implemented through an exquisite disinhibitory circuitry connecting BF SST inhibitory neurons to the VTA DA neurons via the local VTA GABA neurons. Our results reveal a neuronal circuit mechanism underlying prosocial behavior and may provide important information in identifying clinical targets in the treatment of social impairments associated with neuropsychiatric disorders such as schizophrenia and ASDs.

BF SST Neurons Are Required for Prosocial Behavior. The BF has been classically viewed as a brain structure crucial for the regulation of arousal, attention, learning, and memory based on extensive studies of its cholinergic components (24–26). Recently, more diverse brain functions such as fear expression (49, 50), food intake (29, 30, 51), and sleep–wake control (28, 52) have been identified for either cholinergic or noncholinergic subtypes of BF neurons. Here, we found that SST-expressing GABAergic neurons in the BF were robustly activated by diverse social stimuli, including male juvenile, male adult, and female adult mice (Fig. 1 and *SI Appendix*, Fig. S2). Importantly, selective inhibition of these neurons in the BF largely reduced the time of social interaction and even completely abolished social preference
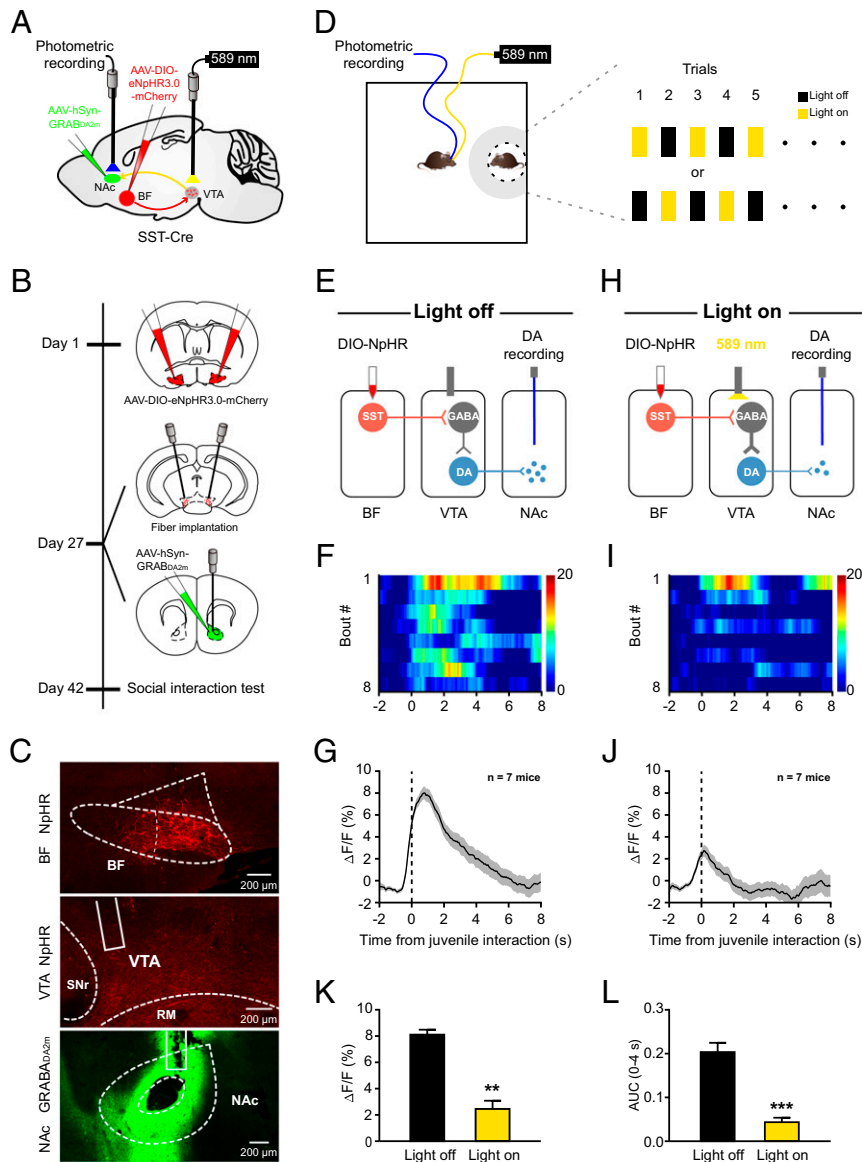
Wang et al.
Basal forebrain mediates prosocial behavior via disinhibition of midbrain dopamine neurons

PNAS | 7 of 10
https://doi.org/10.1073/pnas.2019295118

www.manaraa.com

Fig. 5. Inhibition of BF SST→VTA projections reduces DA release in the NAc during social interaction. (*A*) Schematic illustration of viral injection, fiber implantation, and photometric recording. (*B*) Time course of the experimental design. Day 1: Bilateral injection of eNpHR3.0-mCherry in the BF. Day 27: Bilateral fiber implantation over the VTA for optogenetic inhibition of BF SST→VTA projections; unilateral injection of GRAB$_{DA2m}$ in the NAc and fiber implantation over the NAc for photometric recording. Day 42: Behavioral test. (*C*) Representative images showing NpHR-mCherry expression in the BF (*Top*), NpHR-expressing axon terminals in the VTA (*Middle*), and GRAB$_{DA2m}$ expression in the NAc (*Bottom*), respectively. (*D*) Schematic illustration of photometric recording. Mouse entries into the social zone (gray region: 8-cm vicinity) triggered yellow light to inhibit BF SST→VTA projections in half trials in an alternative fashion. (*E*) Schematic diagram showing photometric recording of NAc DA efflux in light-off trials. (*F*) Heatmap showing GRAB$_{DA2m}$ fluorescence signals aligned to the onset of individual social interaction in light-off trials. Each row represents one bout. The color scale at the right indicates ΔF/F. (*G*) The peri-event plot of the mean GRAB$_{DA2m}$ transient during social interaction in light-off trials for the entire test group (*n* = 7 mice). The thick line indicates mean, and the shaded area indicates SEM. (*H–J*) The same as *E–G* but for light-on trials. (*K* and *L*) Statistical comparison of GRAB$_{DA2m}$ fluorescence signals during social interaction between light-on and light-off trials. Note that inhibition of BF SST→VTA projections significantly reduced both the peak amplitude (*K*) and the AUC (*L*) of GRAB$_{DA2m}$ fluorescence signals. Error bars indicate mean ± SEM, **$P < 0.01$; ***$P < 0.001$; paired *t* test.

in a three-chamber social interaction test (Fig. 2). These findings provide evidence for a causal role of BF SST neurons in the control of prosocial behavior.

In addition to SST neurons, there are three other cell types—that is, cholinergic neurons, PV neurons, and glutamatergic neurons—that populate the BF. Recently, cholinergic neurons along with PV neurons and glutamatergic neurons were found to be wake promoting, whereas SST neurons are sleep promoting (28). Interestingly, consistent with the cell-type-differential regulation of brain functions, we found that glutamatergic neurons were not as active as SST neurons

in response to social stimuli (Fig. 1). Indeed, glutamatergic neurons were only slightly responsive to social stimuli, and the response was comparable to that induced by a toy mouse (Fig. 1). These data suggest that glutamatergic neurons are less likely to play a major role as SST neurons do in gating prosocial behavior. The exact functions of other BF neuronal subtypes, i.e., PV neurons and cholinergic neurons, in regulation of social behavior are to be determined in future studies. However, given the fact that these neuronal populations do not directly target the VTA (36), the neuronal circuit mechanism would be different even if they do have a role in social behavioral regulation.

www.manaraa.com

BF SST→VTA GABA→VTA DA Disinhibitory Circuitry Mediates Prosocial Behavior. The VTA DA neurons play an essential role in regulating social behavior (14, 53). Recently, two elegant studies further demonstrated that projections from the paraventricular hypothalamic nucleus (PVN) and the cerebellum are two upstream inputs to the VTA that are necessary for prosocial interaction behavior (17, 19). Here we identify another upstream input, which originates in the BF, to the VTA that is required for normal social interaction as well (Fig. 3). Notably, there is a major distinction between our newly discovered inputs from the BF to the VTA and those from the PVN or the cerebellum (*SI Appendix,* Fig. S12). In previous studies, both PVN oxytocinergic neurons and cerebellum glutamatergic neurons are excitatory, and they produce direct excitation onto VTA DA neurons and thus increase the activities of DA neurons (17, 19). In contrast, BF SST neurons were not able to directly excite VTA DA neurons given their inhibitory nature. However, they made much more frequent and stronger functional contacts with local VTA GABA neurons than with VTA DA neurons (Fig. 4). As a consequence of such differential innervation patterns, BF SST neurons in principle are able to suppress local GABA neurons and relieve the inhibition that they imposed on DA neurons and thus enhance DA neuron activities. Indeed, optogenetic inactivation of SST neuron axon terminals in the VTA significantly decreased DA release in the NAc, confirming a disinhibitory action of BF SST neurons on VTA DA neurons (Fig. 5). Therefore, distinct from previous findings, the present study reveals a quite unique disinhibitory circuitry by which the activities of VTA DA neurons increase during social behavior.

Importantly, despite the differences in gating mechanisms, optogenetic interference of the disinhibitory circuitry largely abolished the social preference in a three-chamber social interaction test (Figs. 2 and 3). Therefore, the disinhibition produced by BF SST neurons could be as powerful as direct excitation by PVN or cerebellum excitatory inputs in regulation of DA neuron activities and hence of social behavioral output.

Except for the VTA, the LHb is another downstream target that receives dense synaptic inputs from BF SST neurons (*SI Appendix,* Fig. S1) (36). It is well established that the LHb is one key brain region that is associated with negative emotions (54, 55). Intriguingly, recent evidence revealed that this brain structure is also involved in the processing of positive emotions. For example, GABAergic projection from the NAc shell-septum transition zone to the LHb modulates aggression reward (56), and LHb output to the raphe favors social preference (57). Nevertheless, in our study, inhibition of SST neuron axon terminals in the LHb did not have an effect on social behavior (*SI Appendix,* Fig. S7), suggesting that the prosocial effects of BF SST neurons do not seem to involve the LHb-projecting pathway. Therefore, it is likely that BF SST neurons do not uniformly respond to social stimuli and that their prosocial effect is downstream target specific.

The Integration of Multiple Social-Promoting Pathways in the VTA. The VTA receives convergent inputs from a large number of brain regions and serves as a critical node for motivational behaviors including social interaction. The VTA DA neurons integrate these diverse distal inputs and also local GABAergic inputs to generate appropriate firing activities to enable downstream DA release. Growing studies suggest the existence of functionally distinct subpopulations of DA neurons depending on their afferent inputs and/or efferent targets (58–62). It remains unclear how different modes of activity modulation (i.e., excitation vs. disinhibition) are integrated in VTA DA neurons. For example, does the same subpopulation of DA neurons receive both direct excitatory and disinhibitory inputs? Or, alternatively, do different subpopulations of DA neurons receive direct excitatory

and disinhibitory inputs, respectively? These are all important issues worthy of further attention and investigation.

It should be noted that our results do not exclude the possibility that other disinhibitory inputs into VTA DA neurons are involved. Indeed, the biased synaptic connectivity in VTA GABA neurons over DA neurons is also observed in previous studies examining GABAergic inputs from other regions such as NAc, the medial preoptic area (MPO), and the lateral hypothalamus (LH) (63, 64). Moreover, photostimulation of the LH GABAergic projections is sufficient to disinhibit VTA DA neurons and promotes behavioral activation including social interaction (63). Likewise, inhibition of GABAergic projections from either the MPO or the medial NAc shell to the VTA disrupts social preference (64). Consistently, we found that suppression of the MPO→VTA GABAergic projections also substantially attenuated dopamine release in NAc induced by social interaction (*SI Appendix,* Fig. S11). Given this observation, it is conceivable that VTA dopamine neurons need to summate multiple disinhibitory inputs to reach their threshold for phasic firing that is required to trigger high levels of dopamine release and hence prosocial behavior. Inhibiting each of these major inputs could prevent dopamine neurons from reaching their firing threshold and thereby lead to a prominent reduction in dopamine release.

We found that the BF SST GABAergic neurons displayed notable VTA subregion differential innervation, and they targeted mainly the rostral division of the VTA (*SI Appendix,* Fig. S1). This observation is in agreement with a most recent anatomic study showing that long-projection GABAergic inputs often exhibited heterogeneous innervation along the rostral–caudal axis of the VTA (64). For example, GABAergic inputs from the lateral septum predominantly target the VTAR whereas those from the NAc core innervate mainly the paranigral region. Therefore, the diverse disinhibitory inputs could converge on VTA DA neurons located at the same subregion or they could operate through distinct subregions to achieve their social-promoting function. In the end, the disinhibition of VTA DA neurons produced by BF inhibitory inputs would act in concert with disinhibitory inputs from brain regions other than the BF together with multiple direct excitatory inputs. These convergent upstream inputs synergistically tune the DA neuron firing, as well as DA efflux in downstream targets such as the Nac, and consequently contribute to the prosocial behavioral control (*SI Appendix,* Fig. S12).

Materials and Methods

A complete overview of the procedures used in this study can be found in *SI Appendix, Materials and Methods*. This includes information on fiber photometry, optogenetic manipulation, brain slice patch clamp, viral tracing, behavioral tests, and histological analyses.

Animals. Male mice at 2 to 4 mo of age were used. Animal care and use were under the guidelines approved by the Animal Care and Use Committee of Zhejiang University.

Virus Injection. A small volume of virus solution was injected into the target regions at a slow rate.

Fiber Photometry. A fiber photometry system was used to record fluorescence signals emitted by GCaMP6m (a genetically encoded calcium indicator) or GRAB$_{DA2m}$ (an optimized genetically encoded DA sensor).

Animal Behavioral Tests. The overall activity of the test mouse in the apparatus was automatically recorded with a video tracking system (Noldus).

Brain Slice Preparation. Acute brain coronal slices containing the BF, VTA, or LHb were generated using a microtome (Leica VT1200s).

Wang et al.
Basal forebrain mediates prosocial behavior via disinhibition of midbrain dopamine neurons

PNAS | 9 of 10
https://doi.org/10.1073/pnas.2019295118

www.manaraa.com

NEUROSCIENCE

Statistical Analysis. The Student's *t* test or ANOVA was used. Error bars indicate mean ± SEM.

Data Availability. All data are included in the main text or *SI Appendix*.

1. R. Hari, L. Henriksson, S. Malinen, L. Parkkonen, Centrality of social interaction in human brain function. *Neuron* **88**, 181–193 (2015).
2. R. Hari, M. V. Kujala, Brain basis of human social interaction: From concepts to brain imaging. *Physiol. Rev.* **89**, 453–479 (2009).
3. B. Barak, G. Feng, Neurobiology of social behavior abnormalities in autism and Williams syndrome. *Nat. Neurosci.* **19**, 647–655 (2016).
4. D. P. Kennedy, R. Adolphs, The social brain in psychiatric and neurological disorders. *Trends Cogn. Sci.* **16**, 559–572 (2012).
5. L. Brothers, "The social brain: A project for integrating primate behavior and neurophysiology in a new domain" in *Foundations in Social Neuroscience*, J. T. Cacioppo, Ed. *et al.* (The MIT Press, 2002), pp. 367–385.
6. R. Adolphs, The social brain: Neural basis of social knowledge. *Annu. Rev. Psychol.* **60**, 693–716 (2009).
7. R. Adolphs, The neurobiology of social cognition. *Curr. Opin. Neurobiol.* **11**, 231–239 (2001).
8. C. D. Frith, U. Frith, Mechanisms of social cognition. *Annu. Rev. Psychol.* **63**, 287–313 (2012).
9. P. Chen, W. Hong, Neural circuit mechanisms of social behavior. *Neuron* **98**, 16–30 (2018).
10. H. Walum, L. J. Young, The neural mechanisms and circuitry of the pair bond. *Nat. Rev. Neurosci.* **19**, 643–654 (2018).
11. Y. Shemesh *et al.*, Ucn3 and CRF-R2 in the medial amygdala regulate complex social dynamics. *Nat. Neurosci.* **19**, 1489–1496 (2016).
12. D. J. Anderson, Circuit modules linking internal states and social behaviour in flies and mice. *Nat. Rev. Neurosci.* **17**, 692–704 (2016).
13. O. Yizhar *et al.*, Neocortical excitation/inhibition balance in information processing and social dysfunction. *Nature* **477**, 171–178 (2011).
14. L. A. Gunaydin *et al.*, Natural neural projection dynamics underlying social behavior. *Cell* **157**, 1535–1551 (2014).
15. A. C. Felix-Ortiz, K. M. Tye, Amygdala inputs to the ventral hippocampus bidirectionally modulate social behavior. *J. Neurosci.* **34**, 586–595 (2014).
16. G. Dölen, A. Darvishzadeh, K. W. Huang, R. C. Malenka, Social reward requires coordinated activity of nucleus accumbens oxytocin and serotonin. *Nature* **501**, 179–184 (2013).
17. L. W. Hung *et al.*, Gating of social reward by oxytocin in the ventral tegmental area. *Science* **357**, 1406–1411 (2017).
18. M. Murugan *et al.*, Combined social and spatial coding in a descending projection from the prefrontal cortex. *Cell* **171**, 1663–1677.e16 (2017).
19. I. Carta, C. H. Chen, A. L. Schott, S. Dorizan, K. Khodakhah, Cerebellar modulation of the reward circuitry and social behavior. *Science* **363**, eaav0581 (2019).
20. S. Shin *et al.*, Drd3 signaling in the lateral septum mediates early life stress-induced social dysfunction. *Neuron* **97**, 195–208.e6 (2018).
21. G. A. Matthews *et al.*, Dorsal raphe dopamine neurons represent the experience of social isolation. *Cell* **164**, 617–631 (2016).
22. L. L. Oettl *et al.*, Oxytocin enhances social recognition by modulating cortical control of early olfactory processing. *Neuron* **90**, 609–621 (2016).
23. L. Zaborszky, A. Pol, E. Gyengési, "The basal forebrain cholinergic projection system in mice" in *The Mouse Nervous System*, C. Watson, G. Paxinos, L. P. Puelles, Eds. (Academic Press, 2012), pp. 684–718.
24. B. E. Jones, Modulation of cortical activation and behavioral arousal by cholinergic and orexinergic systems. *Ann. N. Y. Acad. Sci.* **1129**, 26–34 (2008).
25. A. Thiele, M. A. Bellgrove, Neuromodulation of attention. *Neuron* **97**, 769–785 (2018).
26. E. C. Ballinger, M. Ananth, D. A. Talmage, L. W. Role, Basal forebrain cholinergic circuits and signaling in cognition and cognitive decline. *Neuron* **91**, 1199–1218 (2016).
27. P. Henny, B. E. Jones, Projections from basal forebrain to prefrontal cortex comprise cholinergic, GABAergic and glutamatergic inputs to pyramidal cells or interneurons. *Eur. J. Neurosci.* **27**, 654–670 (2008).
28. M. Xu *et al.*, Basal forebrain circuit for sleep-wake control. *Nat. Neurosci.* **18**, 1641–1647 (2015).
29. C. Zhu *et al.*, Somatostatin neurons in the basal forebrain promote high-calorie food intake. *Cell Rep.* **20**, 112–123 (2017).
30. J. M. Patel *et al.*, Sensory perception drives food avoidance through excitatory basal forebrain circuits. *eLife* **8**, e44548 (2019).
31. T. Kim *et al.*, Cortically projecting basal forebrain parvalbumin neurons regulate cortical gamma band oscillations. *Proc. Natl. Acad. Sci. U.S.A.* **112**, 3535–3540 (2015).
32. T. L. Kemper, M. L. Bauman, The contribution of neuropathologic studies to the understanding of autism. *Neurol. Clin.* **11**, 175–187 (1993).
33. F. Hoeft *et al.*, Region-specific alterations in brain development in one- to three-year-old boys with fragile X syndrome. *Proc. Natl. Acad. Sci. U.S.A.* **107**, 9335–9339 (2010).
34. A. L. Ciaranello, R. D. Ciaranello, The neurobiology of infantile autism. *Annu. Rev. Neurosci.* **18**, 101–128 (1995).
35. D. Riva *et al.*, Basal forebrain involvement in low-functioning autistic children: A voxel-based morphometry study. *AJNR Am. J. Neuroradiol.* **32**, 1430–1435 (2011).
36. J. P. Do *et al.*, Cell type-specific long-range connections of basal forebrain circuit. *eLife* **5**, e13214 (2016).
37. K. T. Beier *et al.*, Circuit architecture of VTA dopamine neurons revealed by systematic input-output mapping. *Cell* **162**, 622–634 (2015).
38. L. Faget *et al.*, Afferent inputs to neurotransmitter-defined cell types in the ventral tegmental area. *Cell Rep.* **15**, 2796–2808 (2016).
39. L. Vong *et al.*, Leptin action on GABAergic neurons prevents obesity and reduces inhibitory tone to POMC neurons. *Neuron* **71**, 142–154 (2011).
40. H. Taniguchi *et al.*, A resource of Cre driver lines for genetic targeting of GABAergic neurons in cerebral cortex. *Neuron* **71**, 995–1013 (2011).
41. S. S. Moy *et al.*, Sociability and preference for social novelty in five inbred strains: An approach to assess autistic-like behavior in mice. *Genes Brain Behav.* **3**, 287–302 (2004).
42. M. Yang, J. L. Silverman, J. N. Crawley, Automated three-chambered social approach task for mice. *Curr. Protoc. Neurosci.* **Chapter 8**, Unit 8.26 (2011).
43. K. R. Tan *et al.*, GABA neurons of the VTA drive conditioned place aversion. *Neuron* **73**, 1173–1183 (2012).
44. R. van Zessen, J. L. Phillips, E. A. Budygin, G. D. Stuber, Activation of VTA GABA neurons disrupts reward consumption. *Neuron* **73**, 1184–1194 (2012).
45. B. Chieng, Y. Azriel, S. Mohammadi, M. J. Christie, Distinct cellular properties of identified dopaminergic and GABAergic neurons in the mouse ventral tegmental area. *J. Physiol.* **589**, 3775–3787 (2011).
46. S. W. Johnson, R. A. North, Two types of neurone in the rat ventral tegmental area and their synaptic inputs. *J. Physiol.* **450**, 455–468 (1992).
47. R. Lin *et al.*, The raphe dopamine system controls the expression of incentive memory. *Neuron* **106**, 498–514.e8 (2020).
48. F. Sun *et al.*, Next-generation GRAB sensors for monitoring dopaminergic activity in vivo. *Nat. Methods* **17**, 1156–1166 (2020).
49. A. Gozzi *et al.*, A neural switch for active and passive fear. *Neuron* **67**, 656–666 (2010).
50. L. Jiang *et al.*, Cholinergic signaling controls conditioned fear behaviors and enhances plasticity of cortical-amygdala circuits. *Neuron* **90**, 1057–1070 (2016).
51. R. M. Cassidy *et al.*, A lateral hypothalamus to basal forebrain neurocircuit promotes feeding by suppressing responses to anxiogenic environmental cues. *Science Adv.* **5**, eaav1640 (2019).
52. C. Anaclet *et al.*, Basal forebrain control of wakefulness and cortical rhythms. *Nat. Commun.* **6**, 8744 (2015).
53. J. P. Burkett, L. J. Young, The behavioral, anatomical and pharmacological parallels between social attachment, love and addiction. *Psychopharmacology (Berl.)* **224**, 1–26 (2012).
54. P. W. Gold, B. Kadriu, A major role for the lateral habenula in depressive illness: Physiologic and molecular mechanisms. *Front. Psychiatry* **10**, 320 (2019).
55. H. Hu, Y. Cui, Y. Yang, Circuits and functions of the lateral habenula in health and in disease. *Nat. Rev. Neurosci.* **21**, 277–295 (2020).
56. S. A. Golden *et al.*, Basal forebrain projections to the lateral habenula modulate aggression reward. *Nature* **534**, 688–692 (2016).
57. K. Valentinova *et al.*, Morphine withdrawal recruits lateral habenula cytokine signaling to reduce synaptic excitation and sociability. *Nat. Neurosci.* **22**, 1053–1056 (2019).
58. J. W. de Jong *et al.*, A neural circuit mechanism for encoding aversive stimuli in the mesolimbic dopamine system. *Neuron* **101**, 133–151.e7 (2019).
59. W. Menegas, K. Akiti, R. Amo, N. Uchida, M. Watabe-Uchida, Dopamine neurons projecting to the posterior striatum reinforce avoidance of threatening stimuli. *Nat. Neurosci.* **21**, 1421–1430 (2018).
60. S. Lammel *et al.*, Input-specific control of reward and aversion in the ventral tegmental area. *Nature* **491**, 212–217 (2012).
61. H. Yang *et al.*, Nucleus accumbens subnuclei regulate motivated behavior via direct inhibition and disinhibition of VTA dopamine subpopulations. *Neuron* **97**, 434–449.e4 (2018).
62. G. Heymann *et al.*, Synergy of distinct dopamine projection populations in behavioral reinforcement. *Neuron* **105**, 909–920.e5 (2020).
63. E. H. Nieh *et al.*, Inhibitory input from the lateral hypothalamus to the ventral tegmental area disinhibits dopamine neurons and promotes behavioral activation. *Neuron* **90**, 1286–1298 (2016).
64. M. E. Soden *et al.*, Anatomic resolution of neurotransmitter-specific projections to the VTA reveals diversity of GABAergic inputs. *Nat. Neurosci.* **23**, 968–980 (2020).

www.manaraa.com